T. Dudziak*, S. Grobauer, N. Simms, U. Krupp and M. Łukaszewicz

Metal Loss of Steam-Oxidized Alloys after Exposures at 675°C and 725°C for 500 Hours

Abstract: The paper reports metal loss data and general overview of steam oxidation behaviour of the selected alloys in water steam under atmospheric pressure in temperature range of 675–725°C. In this research, T22, T23, TP347HFG, HR3C and 718+ alloys were used. In this study, kinetics and metal loss data were obtained for better understanding corrosion degradation of the exposed materials. All the samples after 500-h exposure were characterized using environmental scanning electron microscopy (ESEM) in backscattered mode (BSE) with energy-dispersive x-ray spectroscopy (EDX). The results indicate that the highest corrosion degradation and metal loss were observed in T22, T23 alloys, moderate degradation was found in TP347HFG, whereas HR3C and 718+ nickel-based alloy showed good corrosion resistance.

Keywords: steam oxidation, metal loss, high temperature, alloy

PACS. 81

DOI 10.1515/htmp-2014-0164
Received September 18, 2014; accepted November 11, 2014

Introduction

In order to secure the energy needs for fast civilization development, the efficiency of coal-fired power plants has to be improved significantly. Steam oxidation of the materials used for boiler components such as superheater and reheater (SH/RH) tubing has become an important research subject due to the increasing demand for a higher steam temperature and pressure, needed to achieve a higher efficiency of pulverized fuel power plants. In this regard, it is crucial to recognize that the energy efficiency of convectional pulverized coal power plant is a strong function of steam conditions; higher steam temperature increases power plant efficiency. However, due to the severity of operational conditions at elevated temperatures, the materials used for the ultra-supercritical (USC) applications have to exhibit better mechanical and physical properties [1]. The existing power plants can be classified as subcritical power plants (560–580°C, steam pressure 140 bar, efficiency around 37%); advanced power plants, with higher operating temperature and pressure (600°C, steam pressure of 280 bar, efficiency 40–45%); USC power plants where steam operating temperatures could reach 760°C with steam pressures of 350 bar and efficiencies of around 60% [2]. Currently in the UK coal-fired power plant boilers operate with ~37% efficiency and with steam temperatures around 560–580°C, where mainly ferritic materials (T22, T23 alloys) with 2–3 wt% of Cr or ferritic-martensitic steels (e.g. T91, T92) with ~9 wt% of Cr are used. Unfortunately, these alloys (especially T22 and T23) show poor high-temperature steam oxidation protection at temperatures above 550°C. In these alloys, thick and non-protective scales are forming [3]. Thus, in order to increase operating temperature of steam in a power plant, it is necessary to use materials with higher Cr contents. Such materials have to form an adherent and a thin protective oxide scale. Alternatively, it is possible to use cheaper materials and accept shorter components life. In this study degradation of materials is shown not only by standard kinetic measurement but additionally through the change in wall thickness (metal loss). Metal loss is a crucial factor highlighting lifetime of the structural materials, especially in the energy sector where reliable materials are fundamental for constant energy supply.

***Corresponding author: T. Dudziak,** Foundry Research Institute, Centre for High Temperature Studies, Zakopianska 73, 30-418, Krakow, Poland, E-mail: tomasz.dudziak@iod.krakow.pl
S. Grobauer, Metallische Konstruktions- und Leichtbauwerkstoffe, Albrechtstr. 30 Raum AC0002, 49009 Osnabrück, Germany, E-mail: sabrinagrobauer@web.de
N. Simms, Foundry Research Institute, Centre for High Temperature Studies, Zakopianska 73, 30-418, Krakow, Poland, E-mail: N.J.Simms@cranfield.ac.uk
U. Krupp, Metallische Konstruktions- und Leichtbauwerkstoffe, Albrechtstr. 30 Raum AC0002, 49009 Osnabrück, Germany, E-mail: u.krupp@hs-osnabrueck.de
M. Łukaszewicz, Foundry Research Institute, Centre for High Temperature Studies, Zakopianska 73, 30-418, Krakow, Poland, E-mail: mikolaj.lukaszewicz@npl.co.uk

Experimental

The materials

In this work five different materials were studied: two ferritic steels T22, T23; two austenitic stainless steels

Table 1: Chemical compositions of the alloys used in this study in wt%.

Alloy	Fe	Cr	C	Si	Mn	P	S	Mo	V	Nb	W	B	Ni
T22	Bal.	2.2	0.1	0.25	0.45	0.0125	0.0125	1	–	–	–	–	–
T23	Bal.	2.2	0.06	0.2	0.46	0.014	0.001	0.08	0.25	0.05	1.54	0.0023	0.14
TP347HFG	Bal.	18.5	0.08	0.75	2	0.04	0.03	–	–	–	–	–	11
HR3C	Bal.	25	0.06	0.4	1.2	–	–	–	–	0.45	–	–	20
718 +	9.47	17.8	0.19	0.4	0.04	0.01	< 0.0003	2.65	0.02	5.5	1.01	0.04	Bal.

HR3C, TP347HFG; and one nickel-based alloy 718 + . The chemical compositions of the alloys are shown in Table 1. Prior to steam oxidation tests at high temperatures, the samples were accurately measured using a digital micrometer (Multico with ± 0.01 μm error). The shapes of the samples used in this study are shown in Figure 1. All surfaces of these tube segments were finished with 600 grit paper ($R_a < 0.4$ μm).

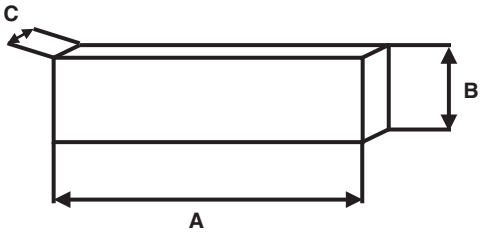

Figure 1: The samples geometry used in high-temperature tests.

Prior to the exposure the samples were cleaned in an ultrasonic bath for 20 min in Volasil followed by rinsing in isopropyl alcohol (IPA), mass gain of the exposed samples was recorded each 100 h.

Oxidation test

Steam oxidation tests at 675°C and 725°C were carried out in the test rig presented in Figure 2. In this type of steam oxidation test facility [4], steam is generated by pumping water from a reservoir into the furnace. Then the steam passes over the test samples and flows into a condenser before the water returns to the reservoir. The water used in the reservoir is double de-ionized. The whole system is sealed and thoroughly purged using oxygen free nitrogen (OFN). This purge continues through the water reservoir throughout the sample exposure period to minimize the level of oxygen in the system [4]. In this study, five cycles, 100 h each at 675°C and 725°C were performed

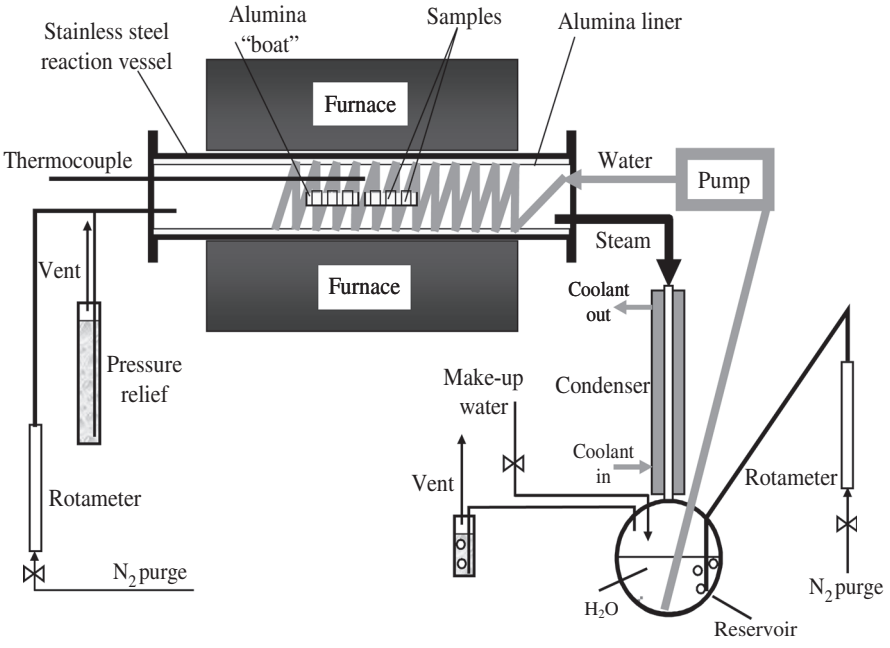

Figure 2: Steam oxidation rig used in this study.

in order to check the performance of the selected alloys. After each 100-h cycle the furnace was cooled down in natural rate due to the power switch off, and the weight of the exposed materials was measured using a digital balance (SATORIUS CP225D) with a resolution of ± 0.01 mg for masses < 80 g. In the test five samples from each alloy were exposed in order to provide better traceability of the corrosion progress. Each individual alloy was removed after each 100 h. The samples were placed on ceramic plates within hot zone, calibrated accurately prior to the experiments at both temperatures.

The balance was calibrated frequently using its internal calibration function and periodically with test weights. Prior to the exposure, furnace calibration was required in order to detect hot zone. The calibration ensured where the best place for the samples was to get the desired test temperature ±5°C. The second test at 725°C was conducted with the same procedure as the 675°C test.

The exposed specimens were metallographically prepared, using cold mounting process. The specimens were placed in moulds that were filled with epoxy resin (Buehler Epoxicure Epoxy, mix ratio: five parts of resin and one part of hardener). The resin needed around 24 h to harden, and then the samples were sliced close to the middle of the sample in a cutting machine (ISOMet 5000). Finally, the samples were ground (on paper 240, 600 and 1200 μm) and polished (Motopol) (using 6 and 1 μm diamond suspension) to enable further investigations, i.e. cross sections.

Metal loss data

The technique for metal loss assessment of the corroded samples was used as a digital image analyser. By comparing sample dimensions before and after the exposure, the apparent change in metal and the change in sound metal (change in metal + internal damage) can be calculated. These data sets can then be re-ordered (from greatest to least metal loss) and corrected for calibration differences (using data from reference samples). Next, the processed data can be plotted as a change in metal vs cumulative probability; effectively, this type of plot indicates the probability (e.g. 4%) of a certain degree of damage being observed, for the data acquisition the software Axio-vision was used. The image analyser is connected with an optical microscope. Figure 3 shows a schematic on the x–y stage for the analysis. 1, Origin; 2, polished cross section; 3, mount; 4, rectangular sample; 5, motorized calibrated X–Y stage.

First of all, a sample is placed on the motorized X–Y stage (cross-sectioned, grinded and polished). An important

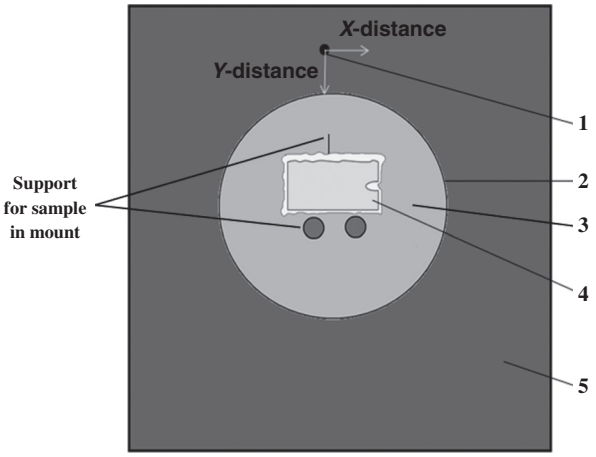

Figure 3: Schematic of a rectangular samples cross section on the digital image analyser stage.

step is to ensure that the long side of specimen is parallel to the x-motion of the stage. After this, the main cross-sectional locations (top, bottom, right and left) on the sample will be fixed. Using these, the machine calculated the x–y co-ordinates around the sample. For the best results ~55 or more points around the sample is required. The images are recorded during measurement, the software automatically made nine individual pictures of each point. Pictures were stitched together and the obvious metal losses in each of these images were pinpointed. Figure 4 demonstrates the function of image analyser (e.g. at point B the x-value = $b2$ and the y value = $a2$). To summarize, in this work the polished cross sections will be all measured using an image analyser to generate accurate measurements of the amount of metal remaining after the corrosion tests; these measurements will be compared to the pre-exposure metal thickness data to produce distributions of the change in metal resulting from the exposures.

Results

Mass change data (kinetics) of the exposed alloys at 675°C and 725°C

Figures below present comparisons of the mass change between the same alloys exposed at two different temperatures. Figure 5 shows mass change data of the samples oxidized in steam: (A) T22, (B) T23, (C) TP347HFG, (D) HR3C and (E) 718+ alloy exposed for up to 500 h at 675°C (solid line) and 725°C (dashed line) in steam oxidation environment T22 alloy exposed at 675°C and 725°C.

The results achieved after steam oxidation test shows that the poorest resistance were shown by T22 and T23

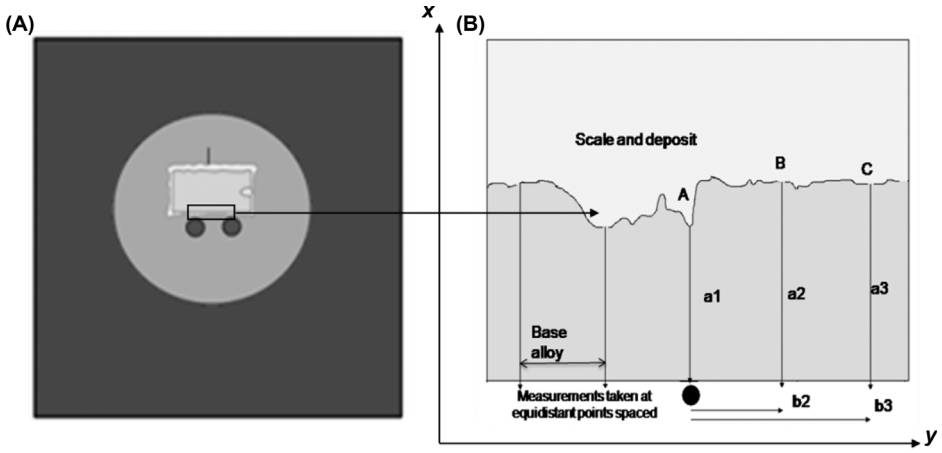

Figure 4: Illustration of function of image analyser. (A) Stage and sample, (B) determining metal loss from the images recorded.

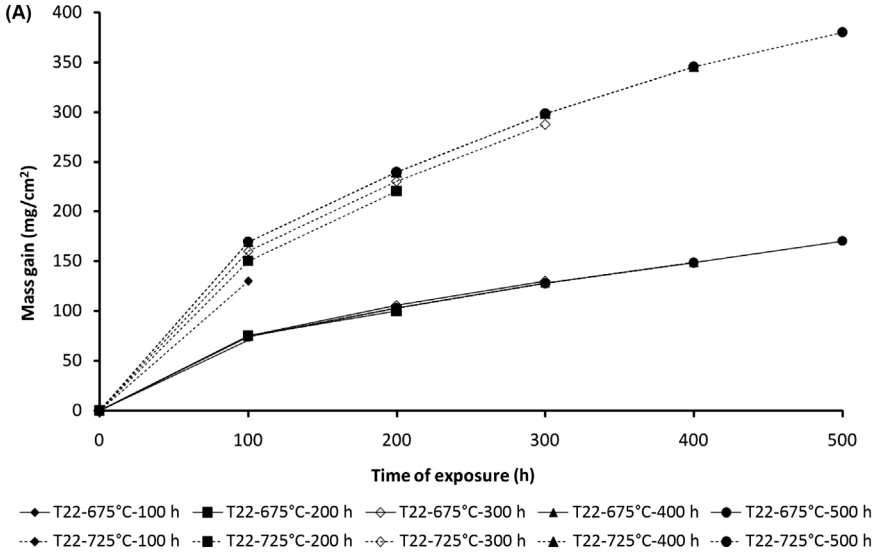

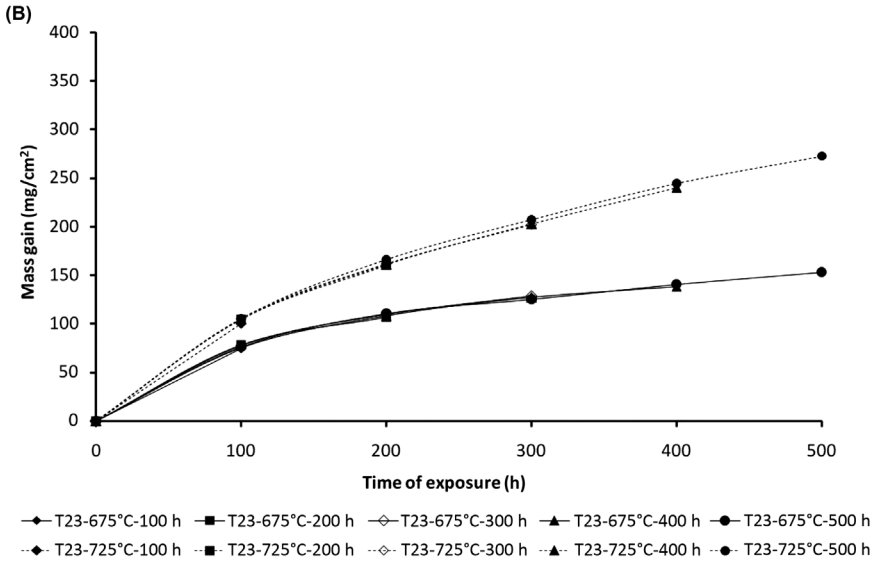

Figure 5: Steam oxidation mass change data: (A) T22, (B) T23, (C) TP347HFG, (D) HR3C and (E) 718 + alloy exposed for up to 500 h at 675°C (solid line) and 725°C (dashed line) in steam oxidation environment.

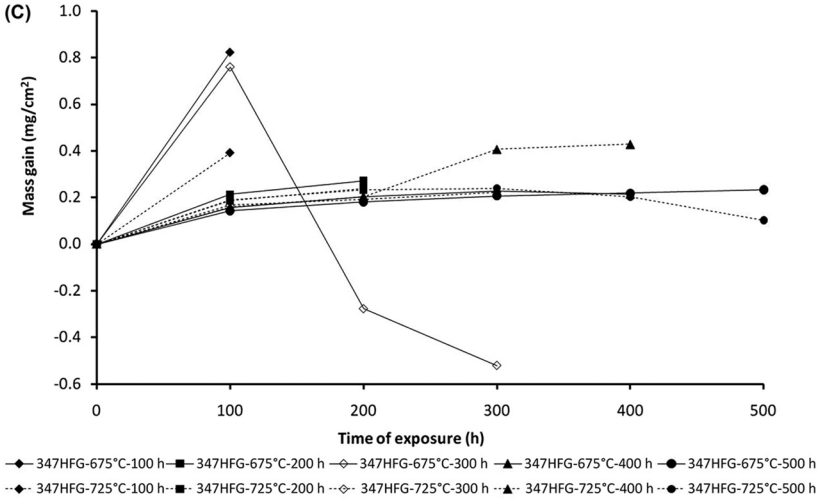

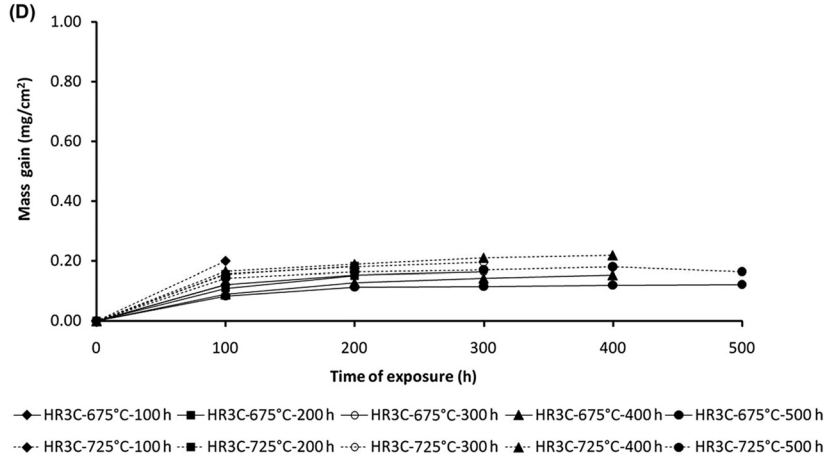

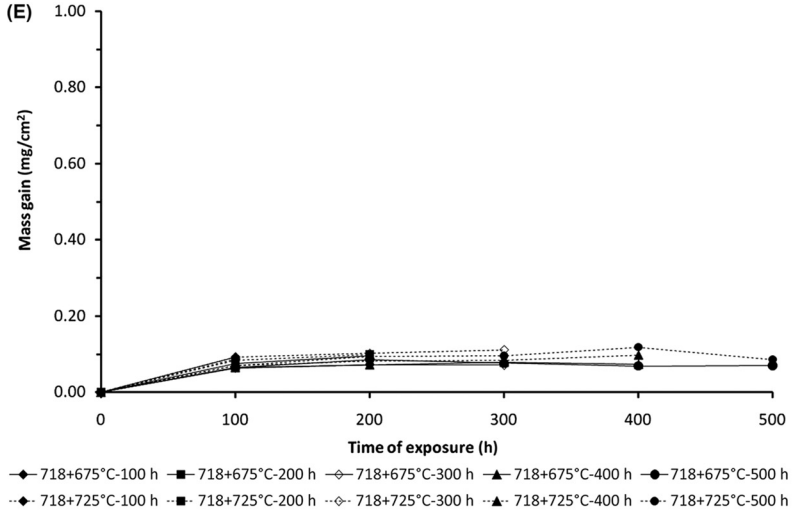

Figure 5: (Continued)

alloys with the lowest Cr content. Both alloys developed non-protective thick oxide scales with good adherence. In comparison to ferritic alloys (T22, T23) mass gain of the austenitic alloys with medium and high Cr content showed much better performance as expected.

It has been found that mass gain of TP347HFG samples in both temperatures showed high degree of instability, where flaky oxide scale spalled off from the material. The observed behaviour probably originates from mismatch of coefficient of thermal expansion (CET) between the formed oxide scale and the substrate. The HR3C alloy showed the formation of protective scale with lack of spallation and good adherence to the bulk material.

Nickel-based alloy 718+ showed the smallest mass gain from all of the exposed alloys due to the formation of protective oxide scale; lack of spallation was observed.

The experimental data points from every test temperature can be reasonably fitted only for two ferritic steels T22 and T23 by a parabolic curve represented by the equation:

$$d^2 = k_p t \quad (1)$$

where d donates the total thickness of the oxide scale and t steam oxidation time. The values of k_p obtained from curve fitting at every temperature are placed in Table 2. Expressing the relationship between the parabolic rate constant and temperature in an Arrhenius type of equation, k_p is given by the following equation [5]:

$$k_p = k_o \exp\left(-\frac{Q}{RT}\right) \quad (2)$$

where Q is the activation energy of steam oxidation, R the gas constant and T the absolute temperature (K). Using the values from the experiment it was possible to determine the specific activation energy Q (kJ/mol) for steam oxidation process. Calculated values of activation energies for T22 and T23 alloys shown the values of −386.1 and −342.9 kJ/mol respectively. The values of activation energy are in good agreement with the other values achieved by other researchers and are shown in Table 3. Aríztegui et al. [6] found that the activation energy for T22 alloy in temperature range subjected to isothermal and non-isothermal oxidation treatments in water steam at several temperatures ranging from 550°C to 700°C for over 1000 h reached −324 kJ/mol.

Table 2: k_p values ($mg^2/cm^4/s$) for the exposed alloys at 657°C and 725°C for 500 h.

Alloy	k_p at 675°C (mg^2/cm^4s)	k_p at 725°C (mg^2/cm^4s)
T22	$5{,}761 \times 10^{-3}$	$6{,}672 \times 10^{-2}$
T23	$3{,}143 \times 10^{-4}$	$4{,}643 \times 10^{-3}$

Table 3: Activation energies (kJ/mol) for T22 and T23 alloys exposed at 657°C and 725°C for 500 h.

Alloy	Activation energy (kJ/mol)
T22	−386.1
T23	−342.9

Microstructural analyses

Surface analysis

This section presents the microstructural analysis of the exposed materials at 675°C and 725°C; it is divided into the surface analysis of ferritic steels (T22 and T23), of austenitic (TP347HFG and HR3C) and Ni-based 718+ alloys. The environmental scanning electron microscopy (ESEM) with energy-dispersive x-ray spectroscopy (EDX) analysis data were obtained after 500 h only.

Exposure at 675°C and 725°C

Figure 6 shows the surface microstructures of the alloys exposed at 675°C and 725°C for 500 h. During the exposure in both temperatures, rough and non-protective oxide was observed in T22 and T23 alloys, the external part of the oxide based on EDX analyses consisted of Fe_2O_3 phase (hematite).

High alloyed steels TP347HFG (~20 wt% Cr) and HR3C (~25 wt% Cr) showed much better corrosion resistance due to the formation of the mixture consisted of Cr–Ni–Fe oxide scales [7]. At 725°C TP347HFG alloy showed a different morphology than that formed after exposure at 675°C; the surface of the material was covered by crystals consisting of Fe–Mn oxides with composition: ~27, ~18 and ~9 wt% of Mn, Fe and Cr, respectively. HR3C alloy at 675°C formed oxide scale with rich content of Cr (~38 wt %), medium content of Fe (~19 wt %), relatively high Mn concentration (6 wt %) and low Ni content was found with concentration of ~2.2 wt %. At higher temperature, HR3C showed very similar behaviour as was shown at 675°C; the developed oxide contained mainly Cr (~35 wt%), Fe (~19 wt%), Mn (~6 wt%) and Ni (~6.5 wt%). The surface of the exposed 718+ sample was covered after 500 h by the layer of the oxide containing ~19 wt% of Cr and ~34 wt% of Ni, in some places Nb-rich crystal formed with following composition: ~55 wt% of Nb, 6.0 wt% of Ni, 3.6 wt% of Co, 12.4 wt% of Cr and 4 wt% of Ti.

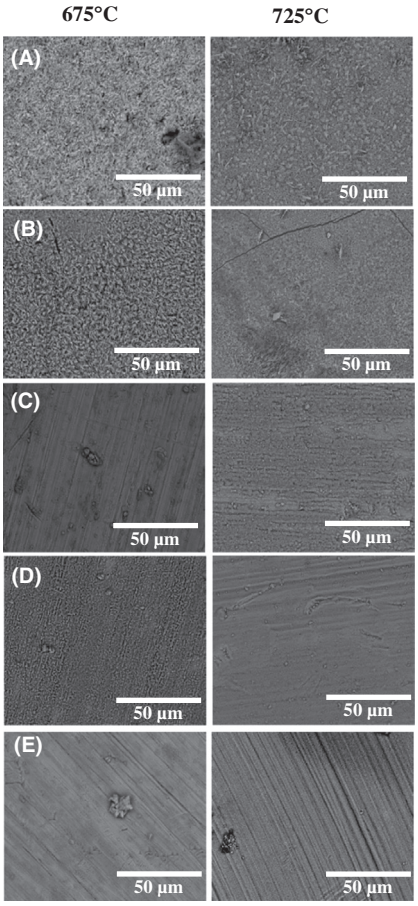

Figure 6: A comparison of the scale morphologies formed on the exposed materials after 500 h at 675°C and 725°C: (A) T22, (B) T23, (C) TP347HFG, (D) HR3C and (E) 718+.

Cross section of exposed materials

The cross-sectioned ESEM images of the exposed materials at 675°C and 725°C in steam environment for 500 h are shown in Figure 7. It needs to be pointed out that EDS concentration profiles are not shown here due to high number of profiles, only overall summary of the outcome of analyses are presented.

T22 alloy showed thicker scale than that observed in T23 alloy after 500 h at 675°C; similar observations were found at higher temperatures. EDX analyses performed on T22 and T23 alloys after exposure showed that the top layer consisted of the phase with 70 wt% of Fe suggesting the formation of Fe_2O_3 (hematite), the middle layer was occupied by the phase with 73 wt% of Fe suggesting development of Fe_3O_4 (magnetite), the phase between the Fe_3O_4 and the substrate consisted of the highest level of Fe suggesting the formation of FeO (wustite) phase. In addition during the exposure of T22 and T23 alloys, in the interface of the oxide scale, enriched region containing up to 5 wt% of Cr and W in T23 was found. Figure 5 shows as well that hematite layer detached from the magnetite layer due to the difference in CTE between both oxides. In contrast, top layer in T23 showed lack of detachment. Both ferritic alloys showed the formation of voids within the developed oxide scale. The voids result from different fluxes of ions with the oxide scale, and different diffusion coefficient with the oxide layers. The voids formation with the oxide scale was discovered and theoretically described by Kirkendall [8]; the effect is enhanced where Fe–Al coating is deposited on Fe-based alloy and heat treated at high temperature [9].

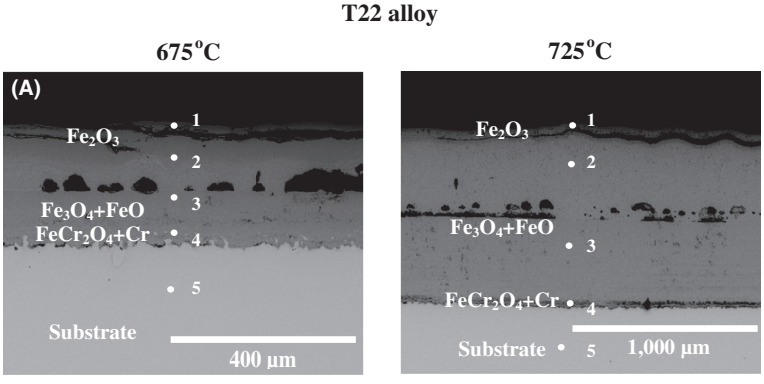

S*	O	Cr	Mn	Fe	Mo
1	27.8	0.5		71.7	
2	26.7	0.6		72.8	
3	24.2	3.1	0.7	70.3	1.7
4		4.4	0.6	93.7	1.3
5		2.3	0.5	97.2	

S*	O	Cr	Mn	Fe	Mo
1	28.2			71.8	
2	25.6		0.6	73.9	
3	24.8	3.9	0.7	70.6	
4	24.1	4.5		69.2	2.3
5		2.2	0.9	96.9	

Figure 7: A comparison of the cross-sectioned samples: after 500-h exposure at 675°C and 725°C: (A) T22, (B) T23, (C) TP347HFG, (D) HR3C and (E) 718+.

T23 alloy

675°C

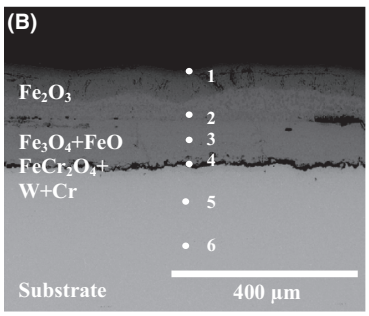

S*	O	Cr	Mn	Fe	W
1	27.7	0.3	0.4	71.5	
2	25.7	0.6		73.8	
3	24.4	3.9		68.0	3.7
4	22.9	4.8		67.7	4.5
5		2.9		94.7	2.4
6		2.7		94.9	2.5

725°C

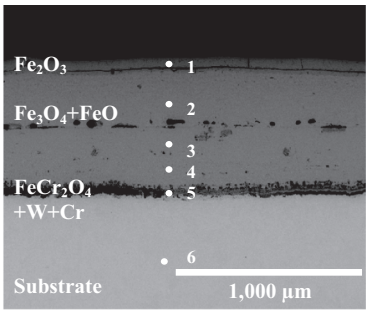

S*	O	Cr	Fe	W
1	29.6		70.4	
2	26.4		73.6	
3	25.3	3.6	67.3	3.8
4	23.8	3.8	69.3	3.1
5	21.2	4.1	70.3	4.3
6		2.5	94.1	3.5

TP347HFG

675°C

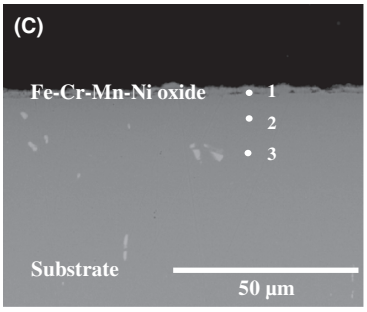

S*	O	Cr	Mn	Fe	Ni
1	18.6	19.8	2.3	51.8	7.6
2		17.4	1.8	70.4	10.4
3		18.2	2.1	69.8	9.8

725°C

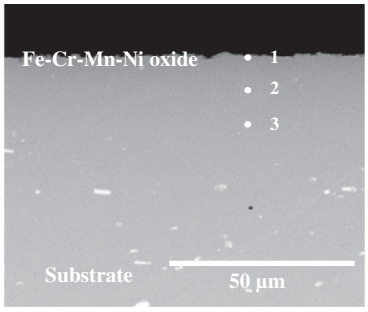

S*	O	Cr	Mn	Fe	Ni
1	2.1	17.4	1.1	69.0	10.4
2		18.9	1.9	69.2	10.0
3		19.4	1.6	69.4	9.6

HR3C alloy

675°C

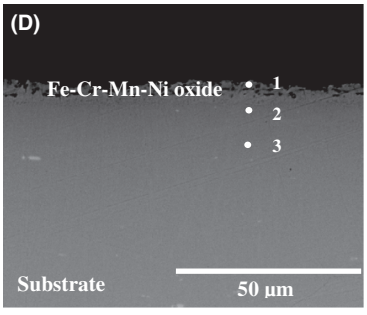

S*	O	Cr	Mn	Fe	Ni
1	10.0	20.9	1.4	49.2	18.6
2		26.7	1.5	51.9	20.0
3		27.1	1.5	51.8	19.6

725°C

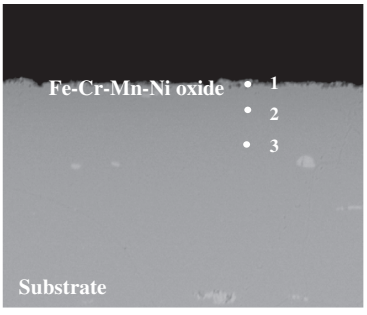

S*	O	Cr	Mn	Fe	Ni
1	2.4	26.1	1.3	51.7	18.5
2		26.7	1.6	52.2	19.5
3		27.2	1.7	51.5	19.6

Figure 7: (Continued)

718+ alloy

675°C

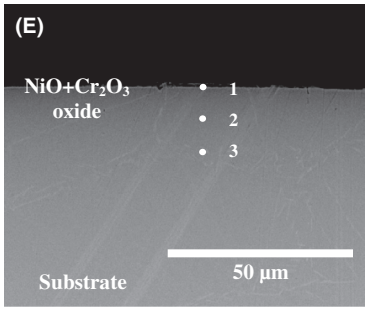

S*	O	Al	Ti	Cr	Fe	Co	Ni	Nb	Mo	W
1	15.7	1.5	0.6	16.8	7.6	7.3	41.0	5.7	3.9	
2		1.7	0.8	18.6	9.4	8.9	51.2	6.3	3.2	
3		1.8	0.7	18.4	9.6	9.2	50.7	6.0	3.7	

725°C

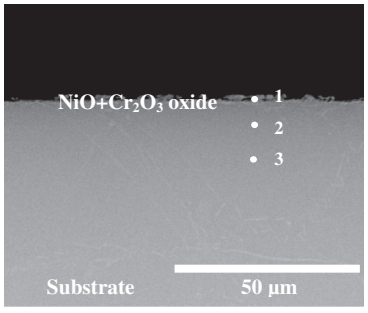

S*	O	Al	Ti	Cr	Fe	Co	Ni	Nb	Mo	W
1	5.6	1.6	1.0	18.2	9.0	8.2	44.2	4.6	3.6	4.0
2		1.7	0.7	18.1	9.2	8.6	48.6	6.3	3.7	3.2
3		1.5	0.9	17.9	9.3	8.7	48.8	5.9	3.5	3.7

Figure 7: (Continued)

Austenitic steels TP347HFG and HR3C alloys formed much thinner oxides as ferritic steels. The formed oxide in TP347HFG alloy at 675°C consisted 51 wt% of Fe, 20 wt% of Cr, 2.5 wt% of Mn and 7.6 wt% of Ni. At higher temperature, according to EDS concentration profiles, Cr reached only 17 wt%, Mn as well showed lower concentration than that found at 675°C. At 725°C higher concentration of Ni was detected in the oxide scale.

The thickness of the oxide scale in both temperatures was relatively low; the thickness was assessed for ~ 2 µm (thickness measurement performed in higher magnification, not shown here). Nevertheless, despite the formation of thin oxide scale, TP347HFG alloy developed as well nodules rich in Fe_3O_4 with Cr addition (not shown here).

Such behaviour was not observed in the alloy with higher content of Cr (HR3C), where thin oxide scale with lack of nodules was formed rich in Cr (20 wt%) and Ni (18 wt%) at 675°C. Further analyses at higher temperature show that the oxide scale formed on HR3C alloy possesses over 26 wt% of Cr and 21 wt% of Ni. Concentration of both Mn and Fe within the oxide scale at both temperatures showed lowered values. Based on these findings, it can be suggested that HR3C alloy showed better corrosion resistance and formation of more protective oxide scale enriched in Cr can be developed at higher temperature. The exposure of 718+ Ni-based alloy developed thin (~1µm) mixture of Ni-Cr oxides with high additions of the other elements (Co, Al and Ti). The alloy showed slightly higher concentration of Cr and Ni at 725 than at 675°C. However, Cr concentration within the oxide scale was much lower than that found in HR3C alloy at both temperatures.

Dimensional metrology of T22 and T23 alloys exposed at 675°C and 725°C

The polished cross sections were all measured using an image analyser to generate accurate assessments of the amount of metal remaining after steam oxidation tests; these measurements were compared to the pre-exposure sample thickness data in order to analyse the distribution

of the change in metal (metal loss) resulting from the exposures. By comparing sample dimensions before and after exposure, the apparent change in metal and the change in sound metal (change in metal + internal damage) can be calculated. These data sets can then be re-ordered (from greatest to least metal loss) and corrected for calibration differences (using data from reference samples). The processed data can then be plotted as a change in metal vs cumulative-probability; effectively, this type of plot indicates the probability (e.g. 4%) of a certain degree of damage being observed. The data can be summarized more readily on cumulative probability plots (for which the data have been ordered from most to least damage). This type of plot highlights the variability of corrosion damage around samples, particularly for the lower Cr content steels. Figure 8 illustrates the change in metal as a function of cumulative probability of T22 and T23 alloys exposed at 675°C and 725°C. In this section only two alloys are presented, T22 and T23, which showed the highest metal loss, significantly exceeding the tolerance of the analyser (5 μm). The other materials (TP347HFG, HR3C and 718+ alloys) showed low metal losses which are very difficult to measure. The results show that the damage levels of the T22 samples was

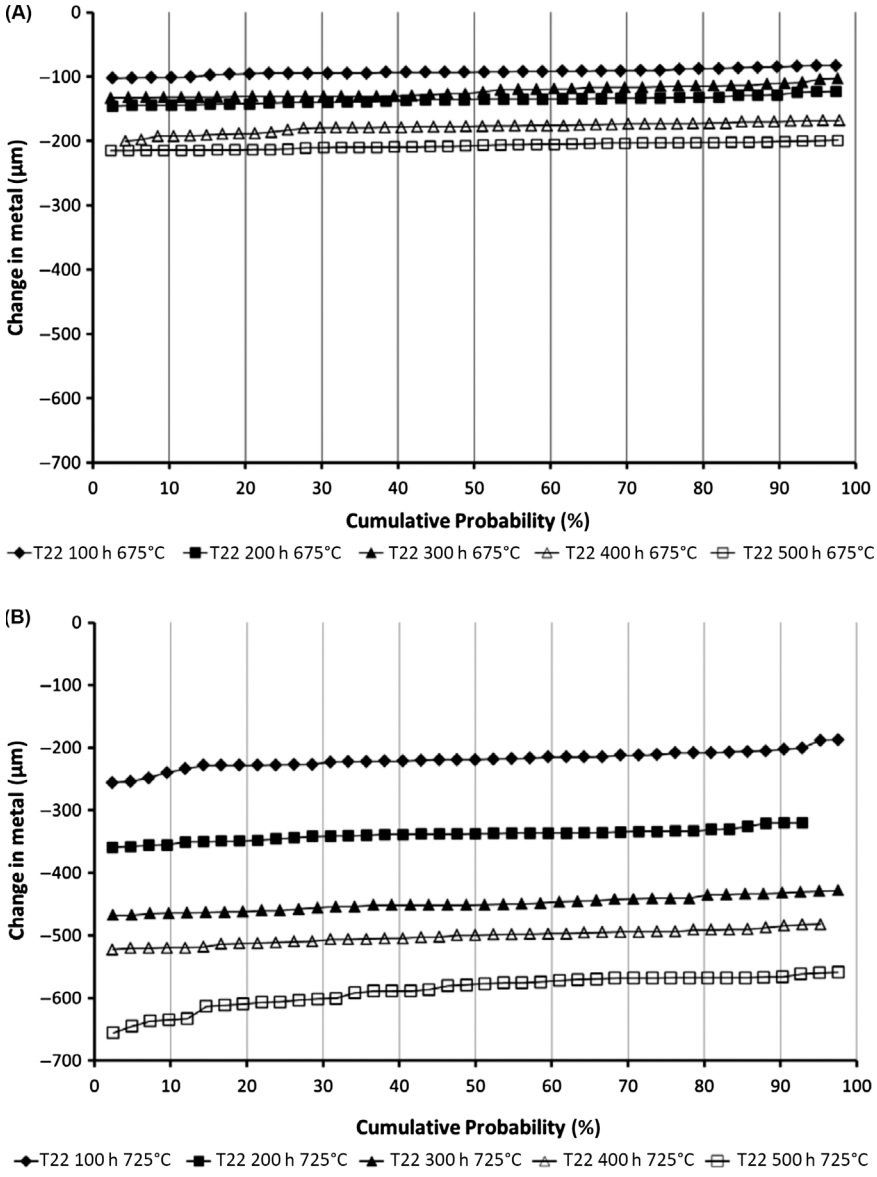

Figure 8: Change in metal vs cumulative probability showing metal loss data of T22 alloy (A and B) and T23 alloy (C and D) after exposure at 675°C and 725°C.

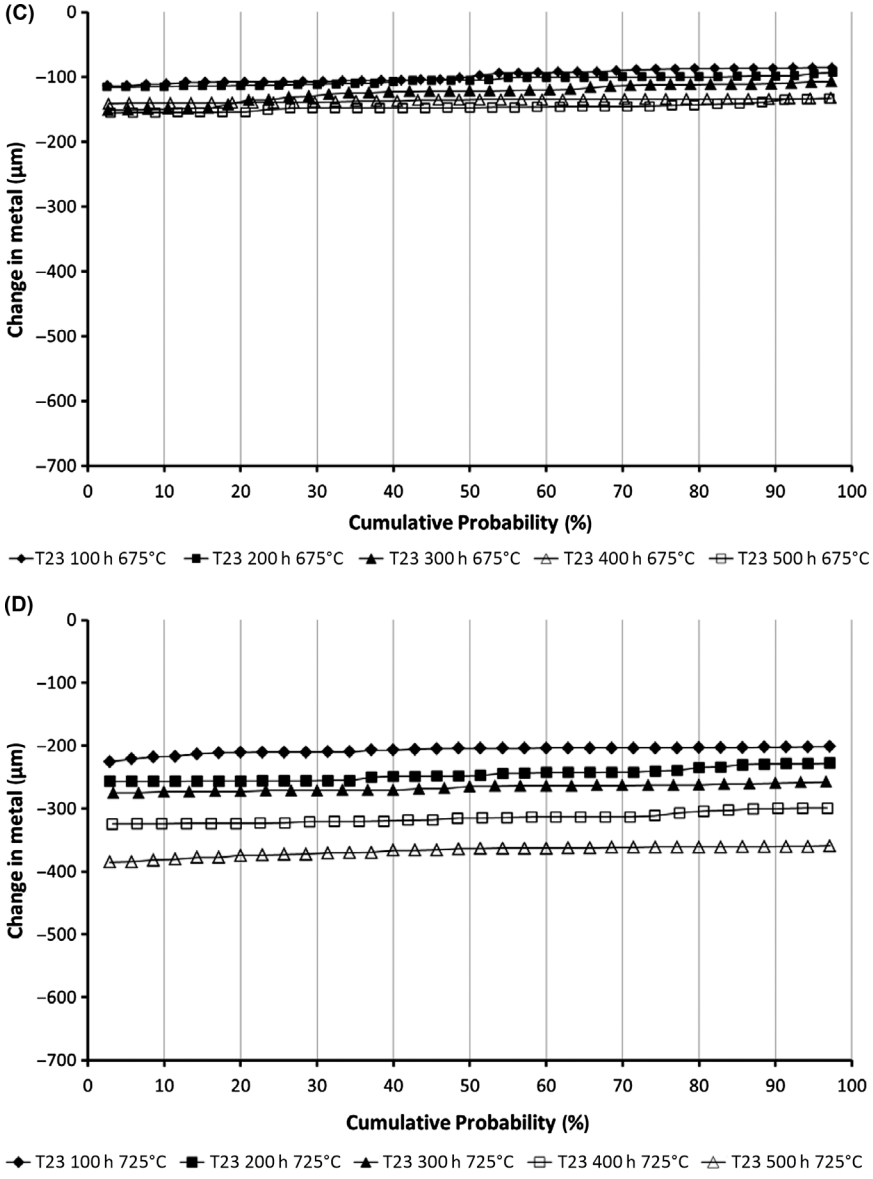

Figure 8: (Continued)

much higher than that observed in T23 material, the metal loss increased with increasing temperature. Median values of metal loss are presented in Figure 9 (A) and (B).

Discussion

The aim of this study was to calculate and show the results of metal loss of the currently useable ferritic steels at high temperature. Additionally, corrosion behaviour of the ferritic steels in steam oxidation was compared with better alloys containing higher Cr content within the matrix. In this study five alloys were taken into consideration: T22, T23, TP347HFG, HR3C and 718+. The two ferritic alloys (T22 and T23) were used in this study to show metal loss of low Cr content materials. Other alloys such as TP347HFG, HR3C and 718+ alloys contained ~19, ~25 and ~18 wt% of Cr, respectively. Due to the different mechanism of the degradation of the exposed alloys in steam environment, the structure of this discussion part is divided into following sections.

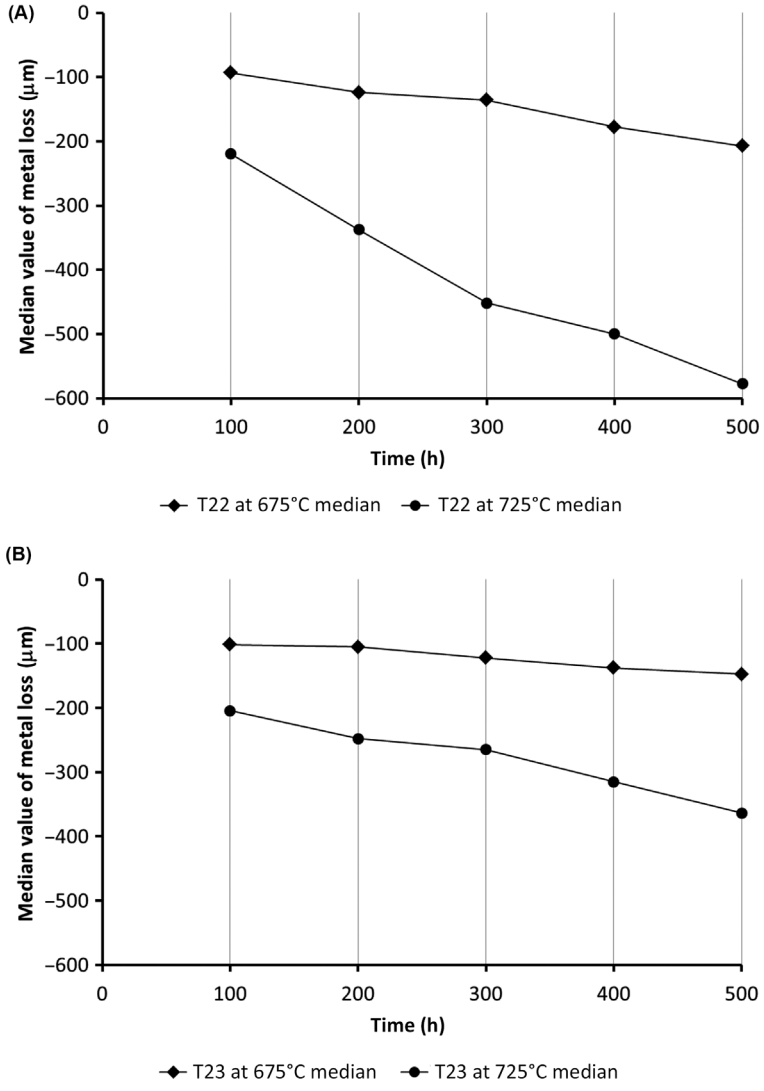

Figure 9: Median values of metal loss of T22 and T23 materials for 500 h at 650°C (A) and 725°C (B).

Steam oxidation behaviour of the ferritic alloys (T22 and T23)

The thickness of the oxide scales formed on T22 and T23 alloys during steam oxidation are not acceptable for components used for boiler components such as SH/RH. The upper limit for the use of these materials is ~580°C, in subcritical power plants with steam pressures of 140 bar [2, 10]. The mechanism of the degradation of T22 and T23 alloys can be demonstrated. Thus when the T22 and T23 alloys are exposed to steam environments, the partial pressure of the oxygen results from the dissociation of steam via following reaction:

$$H_2O(g) \leftrightarrow H_2(g) + \frac{1}{2}O_2(g) \quad (3)$$

The calculated dissociation oxygen partial pressures of steam and the oxides of Fe and Cr as a function of temperature show that the oxygen partial pressure of steam after dissociation is much higher than that needed for the formation of the Fe_2O_3 phase, where Fe_2O_3 is the least stable iron oxide phase.

The formation of Fe_2O_3 in steam environment is often disputed, due to the fact that partial pressure of oxygen after water dissociation is not high enough. However in this work OFN was used that contained 99.998% nitrogen – i.e. an oxygen partial pressure of ~2×10^{-5} atm. This is more than sufficient to oxidize low-alloyed steel and form Fe_2O_3 layer. Moreover, in a well-sealed container, OFN will reduce the dissolved oxygen level in water (and hence steam) to around 20 ppb. Again this is quite sufficient to oxidize reactive metals such as iron.

Thus in steam environment it is likely to observe mainly formation of FeO, Fe_3O_4 and Fe_2O_3 oxides. Grabke et al. [11, 12] described, where five pathways of the oxide growth, as follows:

(1) Outward diffusion of Fe ions, which react with oxygen at the interface (oxide steam), oxygen origin from the dissociation of H_2O at high temperature.
(2) Dissociation of steam at the oxide–steam interface and diffusion of oxygen inward via defects in the oxygen lattice or hydrogen defects. Norby et al. [13] proposed that hydrogen ions entering the oxide lattice could associate with oxygen ions (on their normal lattice sites) to form "hydrogen defects", each of which have an effective charge that would encourage increased cation transport, so increasing the rate of oxide growth and presumably delaying the formation of a more protective layer.
(3) Dissociation of steam on the steam–oxide interface and diffusion of oxygen ions inward to the oxide–alloy interface, reaction with chromium in the alloy, to form internal chromia precipitates.
(4) Steam is transported through the scale; there dissociation of steam occurs (on the oxide–alloy interface) to form iron-chromium oxides. This scenario is unlikely to be possible, unless the formed oxide scale has significant porosity [14].
(5) Dissociation of Fe_3O_4 phase at the interface with the inner and outer layers the released iron ions may diffuse to the oxide–gas interface to react and form new oxide [15].

According to Gala and Grabke et al. [10] the inner layer (Fe_3O_4) dissociates according to the reaction shown below:

$$Fe_3O_4(s) \leftrightarrow 2Fe^{3+} + Fe^{2+} + 4O^{2-} \quad (4)$$

The dissociation of magnetite-released iron ions, which may diffuse outward, and oxygen ions which may diffuse inward in order to form layer of FeO which is more stable at higher temperatures than Fe_3O_4 (magnetite).

The voids in the oxide scale were observed after 500 h of exposure at 675°C and 725°C. Quadakkers et al. [16] showed that the voids formation can be observed on the ferritic oxide scale after long-term exposures. The voids can be unevenly distributed or can coalesce to form a crack or a gap at the interface between the inner and outer layer.

The role of W in low-alloyed steels

Slightly better corrosion resistance of T23 in comparison to T22 can be related to W addition, when added, W through the chemical reaction with C forms WC carbide:

$$W + C \rightarrow WC \quad (5)$$

Thus, due to the higher activity of Cr in T23, more Cr diffuses to the interface where Fe_2CrO_4 spinel can form. In contrast, in low-alloyed steel such as T22, Cr directly reacts with C to form carbides such as Cr_3C_2, Cr_7C_3 and $Cr_{23}C_6$ [17], and significantly decreases Cr activity and concentration, thus much lower amount of Cr diffuses to the interface, as a result thicker non-protective scale based on Fe-oxide can be formed.

Steam oxidation behaviour of TP347HFG alloy

The exposed TP347HFG alloy formed two regions with different degree of the degradation at both temperatures; region with higher degree of resistance formed Fe–Cr spinel with small Ni content. The other region showed a higher degree of the degradation, where small nodules rich in Fe_3O_4 phase with a small amount of Cr formed on the surface. The bottom part of the nodules consisted of Fe_3O_4 with a small amount of Mn.

These findings are in good agreement with the results obtained by the other researchers [7, 19]. The authors of these studies found that the austenitic steels, especially with Cr content lower than 20 wt%, in steam environment are covered by two layers; an outer magnetite layer (Fe_3O_4, sometimes with Fe_2O_3 patches) and an inner layer (Fe–Cr spinel). In this work such structures, as mentioned by the authors, were not observed, however, such morphology can be developed after long exposure time (2,000 h). Thus it can be considered that this model can be fitted to TP347HFG alloy. Otsuka et al. [18] found that after exposure at 700°C for 2,000 h in 1 bar steam pressure, alloys having a lower content of Cr than 20 wt% may develop a relatively uniform layer, with non-formation of healing Cr-rich layer or penetration along alloy grain boundaries. The exposures with longer time cause the formation of irregular thickness developed due to penetration of Cr-rich oxide along alloy grain boundaries.

The behaviour of TP347HFG alloy in steam environment where nodules formed suggests the limited corrosion resistance for a longer period of exposure (10,000 h). According to Quan et al. [19], two mechanisms in nodules formation can be involved:

- Disruption or mechanical failure in an initially formed passive layer with subsequent short-circuit diffusion
- The co-development of two different scale phases from the onset of exposure [20, 21]

The formation of volatile $CrO_2(OH)_2$ phase could as well contribute to the higher rate of degradation of TP347HFG alloy. The volatile chromium oxy-hydroxide $CrO_2(OH)_2$ is formed via [22]:

$$\frac{1}{2}Cr_2O_3(s) + H_2O(g) + \frac{3}{4}O_2(g) \rightarrow CrO_2(OH)_2(g) \quad (6)$$

It is believed that oxygen in eq. (3) comes from dissociation of steam:

$$H_2O \rightarrow H_2 + \frac{1}{2}O_2 \quad (7)$$

Finally, it can be concluded that better steam oxidation resistance of the TP347HFG alloy than T22 and T23 alloys is mainly associated with its higher chromium content (~19 wt%) in the matrix and ability to form protective scale [23]. During these tests at 675°C and 725°C thin layers of Fe–Cr spinel and Fe–Mn spinel have been formed. The development of these phases is a function of temperature, a faster development was observed at higher temperature (725°C) than at lower (675°C).

The formation was associated with a faster diffusion at higher temperature [20]. This statement is in agreement with the findings of Trindade et al. [24] that a low concentration of Cr (17.5 wt%) is required to develop a Cr_2O_3 oxide scale when Fe–Cr alloys exhibit a fine-grained microstructure. In the case of samples with coarse grains (~65 μm), a higher amount of Cr (>17.5 wt%) is required to develop a slow-growing Cr_2O_3 scale as the influence of the grain boundary diffusion is minimized in these materials.

Steam oxidation behaviour of the HR3C alloy

The results obtained here suggest that in order to receive the protective oxide scale, Cr content in the alloy has to be higher than ~17 wt%. Thus in this study HR3C alloy was also exposed. The alloy with ~25 wt% of Cr showed much better corrosion resistance than TP347HFG; the formation of nodules was not observed at 675°C and 725°C after 500 h of exposure. In contrast to TP347HFG alloy, thin protective scale formed, containing mainly Fe-Cr spinel with high amount of Ni (~18 wt%). Thus, the results obtained in this study are in contradiction with the results presented by Otsuka et al. [15], where the alloys with Cr content higher than 20 wt% generally form continuous Cr_2O_3 layers. It is generally accepted that steels containing high levels of Cr have better corrosion resistance, as was mentioned in this work previously. It was observed by Otoguro et al. [25] that the improvements of the alloys with high Cr content in steam oxidation is also caused by high Ni content. The benefit of Ni additions was also reported by Croll et al. [26], who demonstrated the benefit on the oxidation resistance in Fe–Cr–Ni alloys. Caplan et al. [27] also showed that Ni increased oxidation resistance of stainless steels in wet air. It is suggested that this is due to the formation of a Ni-enriched layer.

Steam oxidation behaviour of Ni-based alloy 718+

It was observed that Ni-based alloy 718+ which was exposed at 675°C and 725°C showed the best corrosion resistance in steam oxidation environment from the all exposed alloys. The formation of NiO + Cr_2O_3 or $NiCr_2O_4$ spinel scale was observed. Essuman et al. [28] found that the oxidation of Ni–20Cr in both dry air and wet air resulted in the formation of three oxides. These were Cr_2O_3, NiO and the spinel oxide $NiCr_2O_4$. Whilst in the dry air the NiO phase gradually disappeared with time by reaction with chromia to generate the spinel, in the wet atmosphere, the NiO persisted. Significant cracking and spallation is reported to have occurred after longer exposures at higher temperatures; in this study, the exposed Ni-based alloy showed lack of spallation of the oxide scale.

Similar to Fe-based alloy with medium content of Cr, volatilization of compounds rich in chromium would exert an over-pressure, which would cause the oxide layer to burst. It was found, when chromia layer created continuous layer at the alloy/oxide interface, compressive stresses would be induced causing breakdown of the NiO and $NiCr_2O_4$ layers. The chromia layer is then in contact with the atmosphere and would volatilize as $CrO_2(OH)_2$. Thus from now the exposed alloy depletes in chromium would re-oxidize and a new layer of NiO, and eventually spinel, would develop. It can be suggested that higher content of water vapour in the atmosphere, faster volatilization of Cr can be observed.

It was found in this work, that in some places on the surface during steam oxidation at 675°C and 725°C Nb-rich oxide crystals formed, (~55 wt% of Nb). It can be assumed that the formation of these crystals was due to Nb outward diffusion through the grain boundaries.

Conclusions

The aim of this work was to investigate metal loss degree and steam oxidation behaviour of selected alloys (T22,

T23, TP347HFG, HR3C and 718+) in steam environment at 675°C and 725°C for up to 500 h of exposure. The results obtained in this study clearly show that T22 and T23 ferritic steels showed a similar behaviour, where thick and non-protective Fe oxide scales are formed. The metal loss data from the ferritic steel T22 showed a higher degree of degradation compared with T23 alloy. It is believed that slightly better steam oxidation resistance is driven by the addition of W to T23.

The alloys with higher Cr content (austenitic stainless steels TP347HFG and HR3C and Ni-based alloy 718+) developed a thin and protective oxide layer. The alloy TP347HFG with ~19 wt% of Cr showed Fe_3O_4 nodules formation; on the other hand, the same alloy formed more protective $FeCr_2O_4$ spinel. The alloy HR3C with 25 wt% of Cr showed better oxidation resistance than that observed in TP347HFG, where lack of nodules formation was observed. The alloy developed thin oxide layer of Fe–Cr with high Ni content (18 wt%). Ni-based alloy 718+ due to the formation of a thin oxide scale containing NiO and Cr_2O_3 or $NiCr_2O_4$ spinel showed good steam oxidation resistance at 675°C and 725°C. However, the surface of the alloy was covered by the oxide crystals rich in Nb (~55 wt %).

Acknowledgement: Authors like to acknowledge the support of The Energy Programme, which is a Research Councils UK cross council initiative led by EPSRC and contributed by ESRC, NERC, BBSRC and STFC, and specifically the Supergen initiative (Grants GR/S86334/01 and EP/F029748) and the following companies; Alstom Power Ltd., Doosan Babcock, E.ON, National Physical Laboratory, Praxair Surface Technologies Ltd, QinetiQ, Rolls-Royce plc, RWE npower, Siemens Industrial Turbomachinery Ltd. and Tata Steel, for their valuable contributions to the project.

References

1. Fry TA, Wright IG, Simms NJ, McGhee B, Holcomb GR. Steam oxidation of fossil power plant materials: collaborative research to enable advanced steam power cycles. Mater High Temp 2013;30:261–70.
2. Holcomb RG. Steam turbine materials and corrosion. Albany NY: National Energy Technology Laboratory, 2008.
3. Fry A, Osgerby S, Wright M. Oxidation of alloys in steam environments-a review. London: NPL Materials Centre, 2002.
4. Łukaszewicz M, Simms NJ, Dudziak T, Nicholls JR. Effect of Steam Flow Rate and Sample Orientation on Steam Oxidation of Ferritic and Austenitic Steels at 650 and 700°C. Oxid Met 2013;79:473–83.
5. Laverde D, Gomez-Acebo T, Castro F. Continuous and cyclic oxidation of T91 ferritic steel under steam. Corros Sci 2004;46:613–31.
6. Aríztegui A, Gómez-Acebo T, Castro F. Steam oxidation of ferritic steels: kinetics and microestructure. Bol Soc Esp Cerám Vidrio 2000;39:305–11.
7. Neroth G, Vollenschaar D, der Metalle DK. Wendehorst Baustoffkunde 2011:735–49. http://www.springerprofessional.de/978-3-8348-9919-4---wendehorstbaustoffkunde/1808484.html
8. Smigelskas AD, Kirkendall EO. Zinc Diffusion in Alpha Brass. Trans AIME 1947;171:130–42.
9. Fan DW, Kim HS, Oh JK, Chin KG, De Cooman BC. Influence of isothermal deformation conditions on the mechanical properties of 22MnB5 HPF steel. ISIJ Int 2010;50:561–8.
10. Dooley RB. Program on technology innovation: oxide growth and exfoliation on alloys exposed to steam. Palo Alto, CA: EPRI, 2007.
11. Gala A, Grabke HJ. Arch Eisenhüttenwes 1972;43:463–9.
12. Grabke HJ, Viefhaus H. Phys Chem 1980;84:152–9.
13. Norby T. Hydrogen defects in inorganic solids. O. Johannessen, AG Andersen, editors. Amsterdam: Elsevier, 1989.
14. Mayer P, Manolescu AV. Proceedings of international corrosion conference series NACE-6, Houston, 1983:368–379.
15. Wright IG, Wood GC. The isothermal oxidation of Co-Cr alloys in 760 Torr oxygen at 1000°C. Oxid Met 1977;11:163–91.
16. Quadakkers W. Mechanisms of Steam Oxidation in High Strength Martensitic Steels. Int J Pres Ves Pip 2007;84:75–81.
17. Ellis J, Haw M, Carbides C. Wear Resistant Coatings. Mater World 1997;5:1–36.
18. Otsuka N, Fujikawa H. Scaling of Austenitic Stainless Steels and Nickel-Base Alloys in High-Temperature Steam at 973 K. Corrosion 1991;47:240–8.
19. Quan NS, Young DJ. Sulfidation behavior of an aluminum-manganese steel. Oxid Met 1986;25:107–19.
20. Sakiyama M, Tomasazewicz P, Wallwork GR. Oxidation of iron-nickel aluminum alloys in oxygen at 600–800°C. Oxid Met 1979;13:311–30.
21. Smith PJ, Beauprie RM, Smeltzer WW, Stevanovic DV. The effect of aluminum ion implantation on the oxidation of an Fe-6 at.% Al alloy at 1173 K. Oxid Met 1987;28:259–76.
22. Wright I, Dooley R. A review of the oxidation behaviour of structural alloys in steam. Philadelphia, PA: Maney for the Institute and ASM International, 2010.
23. Wright I, Pint B. Proceedings of the NACE conference, August 8–11, 2002, Denver, 2002.
24. Trindade VB, Krupp U, Wagenhuber E-G, Christ H-J. Oxidation Mechanisms of Cr-Containing Steels and Ni-Base Alloys at High Temperatures – Part I: The Different Role of Alloys Grain Boundaries. Mater Corros 2005;56:785–90.
25. Otoguro Y, Sakakibara M, Saito T, Ito H, Inoue Y. Corrosion behaviour of austenitic heatresisting steels in a high temperature and high pressure steam environment. Trans ISIJ 1988;28:761–8.

26. Croll JE, Wallwork GR. The high-temperature oxidation of iron-chromium-nickel alloys containing 0–30% chromium. Oxid Met 1972;4:121–40.
27. Caplan D, Cohen M. Influence of Impurities on the Oxidation of Fe-26Cr Alloys. Nature 1965;205:690–702.
28. Essuman E, Walker LR, Maziasz PJ, Pint BA. Oxidation behaviour of cast Ni–Cr alloys in steam at 800°C. Mater Sci Tech 2013;29:822–7.

Notes: Work carried out at Centre for Energy and Resource Technology, Cranfield University, Bedfordshire MK43 0AL, UK.
T. Dudziak: Currently employed at Foundry Research Institute, Centre for High Temperature Studies, Zakopiańska 73, 30–418 Krakow, Poland.
M. Łukaszewicz: Currently employed at National Physical Laboratory, Hampton Rd, Teddington, Middlesex TW11 0LW, UK.